Porosity governs normal stresses in polymer gels

De Cagny, H.C.G.; Vos, B.E.; Vahabi, M.; Kurniawan, N.A.; Doi, M.; Koenderink, G.H.; MacKintosh, F.C.; Bonn, D.

DOI
10.1103/PhysRevLett.117.217802

Publication date
2016

Document Version
Other version

Published in
Physical Review Letters

Porosity governs normal stresses in polymer gels
Supplementary Information

Henri C. G. de Cagny[*a], Bart E. Vos[*b], Mahsa Vahabi[*c], Nicholas A. Kurniawan[b,d], Masao Doi[e], Gijsje H. Koenderink [†b], Fred C. MacKintosh [‡c,f], and Daniel Bonn [§a]

[a]Institute of Physics, University of Amsterdam, Amsterdam, The Netherlands
[b]FOM-Institute AMOLF, Amsterdam, The Netherlands
[c]Department of Physics and Astronomy, Vrije Universiteit, 1081HV Amsterdam, The Netherlands
[d]Department of Biomedical Engineering & Institute for Complex Molecular Systems, Eindhoven University of Technology, Eindhoven, The Netherlands
[e]Center of Soft Matter Physics and its Applications, Beihang University, Beijing, China
[f]Departments of Chemical & Biomolecular Engineering, Chemistry, and Physics & Astronomy, Rice University, Houston, 77005 TX

Materials and Methods

Chemicals were purchased from Sigma Aldrich (Zwijndrecht, the Netherlands). Human plasma fibrinogen and thrombin were purchased from Enzyme Research Laboratories (Swansea, United Kingdom). Fibrinogen stock solution was diluted to 8 mg/mL in assembly buffer (150 mM NaCl, 20 mM HEPES and 5 mM $CaCl_2$) at a pH of 7.4. Dense networks (fine clots) with an average pore size of 0.08 μm were obtained in fine-clot assembly buffer (400 mM NaCl and 50 mM Tris-HCl) at a pH of 8.5 [1]. The mixtures were prewarmed to the desired polymerization temperature and 0.5 U/mL thrombin was added to initiate network formation. The fibrin gels were allowed to polymerize *in situ* for at least 12 hours (22°C and 27°C samples) or 4 hours (37°C samples) between the prewarmed cone and plate geometry of an Anton Paar rheometer (Physics MCR 302, Graz). Polyacrylamide gels were polymerized by preparing a mixture of polyacrylamide and N,N'-methylenebis(acrylamide)(Bis) followed by dilution to the desired final concentration. Polymerization was initiated by adding ammonium persulfate (0.5 μg/mL) and tetramethylethylenediamine (1 μL/mL) and allowed to proceed in situ between the rheometer plates at 20 °C. We used a 40 mm, 2° stainless steel cone-plate geometry for all fibrin data and a 50 mm, 2° stainless steel cone-plate geometry for polyachrylamid data reported in the main text, and a series of stainless steel cone-plate and plate-plate geometries in additional experiments reported in the Supplementary Information. Solvent evaporation was prevented by adding a layer of mineral oil (Sigma Aldrich, M3516) to cover the liquid-air interface. We checked that this procedure did not influence the normal stress response. The composition of the polyacrylamide gels displayed in Figure 1a of the main text are the following:

Gel	Total polymer mass fraction (%)	Acrylamide-MBAA mass ratio
A	4	149:1
B	5	199:1
C	4	99:1
D	6	299:1
E	3	39:1

[*]authors contributed equally
[†]Email: g.koenderink@amolf.nl
[‡]Email: fcmack@gmail.com
[§]Email: d.bonn@uva.nl

We measured the linear elastic shear modulus G of the gels by measuring the stress response to a small oscillatory shear strain with an amplitude of 0.1% and frequency of 1 Hz. The normal stress response to an applied shear was obtained by applying Large-Amplitude Oscillatory Shear (LAOS) at a range of frequencies (0.001 Hz to 7 Hz) at a shear stress amplitude of 800 Pa. We measured the time-resolved strain and normal stress response using an oscilloscope coupled to the analogue outputs of the rheometer. The characteristic normal-stress relaxation time was obtained by applying a constant shear stress (400 Pa for the 22 °C and the 27 °C gels, 550 Pa for the 37 °C gel, 500 Pa for the fine clot gel and a strain of 150% for PAAm). The relaxation data for PAAm were smoothed using Savitzky-Golay filter. The relaxation stress experiment was initiated one day after the polymerization to ensure the stability of the base line

To characterize the pore size of the fibrin gels, we performed light scattering measurements using a spectrophotometer (Lambda35 UV/VIS Perkin Elmer, Waltham, MA, USA). Gels were polymerized in quartz cuvettes and absorbance spectra were taken over a wavelength range from 450 to 900 nm. The mass-length ratio of the fibers was obtained by fitting the spectra to a scattering model that assumes a random network of rigid cylindrical fibers [2, 3]. The average mesh size $\xi \sim \sqrt{1/\rho}$ follows from the fiber length density $\rho = \frac{\mu}{c_p}$, where μ is the fiber mass-length ratio and c_p the fibrinogen concentration. To validate the light scattering measurements, we also performed image analysis of confocal fluorescence microscopy images of fibrin networks doped with 5 mole% AlexaFluor 488-conjugated fibrinogen (Life Technologies, Eugene, Oregon, USA). Images were obtained on a Nikon Eclipse TI confocal system with a 100x oil immersion objective (NA=1.40). Image analysis is discussed in the Supplementary Information section 'Pore size analysis'.

Two-fluid model and relaxation of hoop stress

When an elastic body is sheared by twisting, either in the classic wire experiments of Poynting or in a conventional cone-plate or parallel plate rheometer, sections of the material tend to be stretched out circumferentially. The resulting sections also tend to develop tensile stresses as they are stretched out. Through the combination of tension and the curved shape, these tensile hoop stresses result in a net inward radial force, much as a curved rubber band would when stretched into a circular shape. These effects contribute to a net stress $\tilde{\sigma}$ and radial force, proportional to the curvature of the streamlines, tending to drive inward contraction of the gel. By symmetry, this force must be even in the applied strain, since the tension is independent of the direction of rotation of the rheometer. Thus, to lowest order, a quadratic dependence on shear strain γ is expected. We define this force (per unit volume) to be

$$f_r = -\frac{\tilde{\sigma}}{r} \simeq -\frac{1}{r}\tilde{A}G\gamma^2, \tag{1}$$

where the coefficient $\tilde{A}$ is dimensionless. In an incompressible medium, in which net radial motion is not possible, this radial force must be balanced by a pressure that builds toward the axis of the rheometer. In the presence of a free surface, as opposed to a rheometer plate, this gives rise to rod-climbing behavior. In the case of a rheometer, the pressure results in a positive, upward thrust F.

For a polymer gel consisting of both network and solvent, radial motion of the network is possible, which can lead to a relaxation of the pressure contribution to the measured thrust. To model this relaxation, we use the two-fluid model [4–7], in which the network displacement u and solvent velocity v satisfy the coupled equations. The equation for the net force per unit volume acting on the fluid in the non-inertial limit is

$$0 = \eta\nabla^2\vec{v} - \vec{\nabla}P - \Gamma\left(\vec{v} - \dot{\vec{u}}\right), \tag{2}$$

while the corresponding (non-inertial) equation for the force on the network is

$$0 = G\nabla^2\vec{u} + (G+\lambda)\vec{\nabla}\cdot(\vec{\nabla}\cdot\vec{u}) + \Gamma\left(\vec{v} - \dot{\vec{u}}\right), \tag{3}$$

where η is the solvent viscosity, G is the shear modulus and λ is a Lamé coefficient that is typically of order G. These equations are coupled by a term representing the force on the fluid (and opposite to the force on the network) due to the relative motion of the two components. The coupling constant Γ is expected to be of order η/ξ^2 for a network mesh size ξ. This can be estimated in a free-draining approximation by considering the drag force on a network strand of length $\sim \xi$ moving with velocity $\dot{\vec{u}}$ with respect to a stationary solvent. Apart from a weak logarithmic correction, this drag force is approximately $4\pi\xi\eta\dot{u}$. This is the force per mesh volume $\sim \xi^3$, meaning that the force per unit volume is of order $\eta\dot{u}/\xi^2$. This is the net force per unit volume on the fluid given by the last term on the right-hand side of (2) with $\vec{v} = 0$.

If the volume fraction of the network is small, as it is for most biopolymer gels ($\sim 10^{-3}$), then we can safely assume that only the network moves radially in response to strain-induced hoop stresses $\tilde{\sigma}$, while the solvent remains stationary since it is incompressible. In this case, the radial component of (2) reduces to $\nabla_r P = \Gamma \dot{u}_r$. Again, the radial motion of the network at low volume fraction is well approximated by

$$\Gamma \dot{u}_r \simeq G \frac{\partial^2}{\partial z^2} u_r. \tag{4}$$

Here, we have assumed a cone-plate geometry with gap $d \ll r$. Corrections to (4), from both $\nabla^2 \vec{u}$ and $(G+\lambda)\vec{\nabla}\cdot(\vec{\nabla}\cdot\vec{u})$ terms are smaller by of order $(d/r)^2$. Together with the boundary conditions that $u_r = 0$ at both $z = 0$ and $z = d$, we find a characteristic relaxation time

$$\tau \propto \frac{\Gamma d^2}{G} \sim \frac{\eta d^2}{G\xi^2} \tag{5}$$

for the radial motion with axial profile $u_r \propto \sin(\pi z/d)$. The simplified linear equation of motion is

$$\Gamma \dot{u}_r \simeq -(\pi^2 G/d^2) u_r. \tag{6}$$

What is still missing from this analysis is the additional force in (1) acting on the network due to hoop stresses. Being fundamentally nonlinear, this is not captured by (3), so we add this to the results of the (linear) two-fluid model to obtain the following phenomenological equation of motion:

$$\nabla_r P = \Gamma \dot{u}_r = -K \frac{u_r}{r^2} - \frac{1}{r} \tilde{A} G \gamma^2. \tag{7}$$

Here, $K \simeq \pi^2 G/\tan(\alpha)^2$ and we have used the fact that $d = \tan(\alpha)\, r$. Importantly, this is a linear equation of motion for u_r, in spite of the $\sim \gamma^2$ driving force. The latter is controlled by the rheometer and acts as in inhomogeneous term in an otherwise linear differential equation for the unknown $u_r(t)$.

Incompressible limit

First, let's consider the case of an incompressible medium, as one has for the limit $\Gamma \to \infty$, where $u \to 0$ and

$$\nabla_r P = -\frac{1}{r} \tilde{\sigma}. \tag{8}$$

This equation can be integrated to give

$$P(R) - P(r) = -\tilde{\sigma} \log(R/r), \tag{9}$$

where $P(R)$ is the pressure at the sample boundary, i.e., atmospheric pressure P_0. The excess pressure,

$$\Delta P = P(r) - P_0 \tag{10}$$

can be integrated to give a positive (upward) contribution to the thrust F

$$2\pi\tilde{\sigma} \int_0^R r \log(R/r) dr = \frac{\pi R^2}{2} \tilde{\sigma}. \tag{11}$$

Adding this to the direct contribution

$$-\pi R^2 \sigma_{zz} \tag{12}$$

from σ_{zz}, we find that

$$\frac{2F}{\pi R^2} = N_1 = \sigma_{xx} - \sigma_{zz}, \tag{13}$$

implying that,

$$\tilde{\sigma} = \sigma_{xx} + \sigma_{zz} \simeq \tilde{A} G \gamma^2, \tag{14}$$

where $\tilde{A} = (A_x + A_z)$,

$$\sigma_{xx} \equiv A_x G \gamma^2 \quad \text{and} \quad \sigma_{zz} \equiv A_z G \gamma^2. \tag{15}$$

We expect $A_z \sim 1/\gamma_0$, based on the prior low-frequency model [8, 9]. Since σ_{xx} usually is of order but larger than σ_{zz}, we expect both $A_{x,z} \sim 1/\gamma_0$, which is typically of order 10 for biopolymer networks. Moreover, as defined both stress components are strictly positive (tensile) and we expect that $A_x > A_z$, for $N_1 > 0$ in the incompressible limit.

Compressible limit

In the limit of long times $t \gg \tau$ and low frequencies $\omega\tau \ll 1$ in Eq. (7), the pressure vanishes, and the apparent N_1 measured is that of Refs. [8, 9]

$$\frac{2F}{\pi R^2} = N_1^{\rm app} = -2\sigma_{zz} = -2A_z G\gamma^2. \tag{16}$$

This describes the long-time value in Fig. 2c of the main text, to which the normal stress relaxes. For intermediate times/frequencies, we solve Eq. (7), with $\gamma(t) = \gamma_0 \sin(\omega t)$, to find both steady-state (ss) and transient (tr) solutions, where the general $u_r(t) = u^{(\rm ss)}(t) + u^{(\rm tr)}(t)$. We find

$$u^{(\rm ss)}(t) = -\frac{\tilde{A}G_0\gamma_0^2 r\left(-K^2\cos(2t\omega) + K^2 - 2\Gamma K r^2\omega\sin(2t\omega) + 4\Gamma^2 r^4\omega^2\right)}{2\left(K^3 + 4\Gamma^2 K r^4\omega^2\right)} \tag{17}$$

and

$$u^{(\rm tr)}(t) = \frac{\tilde{A}G_0\gamma_0^2 r}{2K\left(\frac{K^2}{4\Gamma^2 r^4\omega^2}+1\right)} e^{-\frac{K}{\Gamma r^2}t}. \tag{18}$$

The transient is found by choosing a homogeneous solution of (7) to give $u_r(t) = u^{(\rm ss)}(t) + u^{(\rm tr)}(t) = 0$ at $t = 0$. The transient is most relevant to the case where its characteristic relaxation time τ is large compared with the period of oscillation $\sim 1/\omega$. Thus, we approximate

$$u^{(\rm tr)}(t) \simeq \frac{\tilde{A}G_0\gamma_0^2 r}{2K} e^{-\frac{K}{\Gamma r^2}t}, \tag{19}$$

from which we find

$$\nabla_r P = \Gamma\dot{u}_r \simeq -\frac{\tilde{A}G_0\gamma_0^2}{2r} e^{-\frac{K}{\Gamma r^2}t}. \tag{20}$$

As noted before, there is no single relaxation time in this system, since $\tau \sim \eta d^2/(G\xi^2)$ depends on the gap d. This can be seen in (20), where the relaxation is r-dependent. This can be integrated to find the transient contribution to $N_1^{\rm app}$ given by

$$N_1^{\rm transient} \simeq \frac{1}{2}\tilde{A}G_0\gamma_0^2\left(\frac{{\rm Ei}\left(-t/\tau\right)t}{\tau} + e^{-t/\tau}\right) \simeq \frac{1}{2}\tilde{A}G_0\gamma_0^2\exp\left[-1.91\left(\frac{t}{\tau}\right)^{0.78}\right], \tag{21}$$

where the latter approximation is valid to within less than 2% until the transient has decayed to less than 2% of its initial value.

For the steady-state,

$$N_1^{\rm app} = -2A_z G\gamma^2 + \tilde{A}G\gamma_0^2\left(\mathcal{A}\cos(2\omega t) + \mathcal{B}\sin(2\omega t)\right), \tag{22}$$

where

$$\mathcal{A} = -\frac{1}{8\omega\tau}\left[2\tan^{-1}\left(1+2\sqrt{\omega\tau}\right) + 2\tan^{-1}\left(1-2\sqrt{\omega\tau}\right) - \pi + 4\omega\tau\right] \tag{23}$$

and

$$\mathcal{B} = \frac{1}{8\omega\tau}\log\left(1+4\omega^2\tau^2\right). \tag{24}$$

For an incompressible system, (13) is recovered for $u_r(t) = u^{(\rm ss)}(t) + u^{(\rm tr)}(t)$ as $\tau \to \infty$. In the limit of low frequency, this reduces to the fully compressible limit of (16).

Application of the model to the experimental results

The experiments are done on fibrin samples with different mesh sizes, obtained by varying the temperature, ionic conditions and pH. To explain the experimental results using the two-fluid model, we fit the steady state normal stress data to Eq. (22). The free parameters in this equation are A_z and $\tilde{A}$. In this formula ω is the frequency of oscillatory shear stress or strain. The other parameters G, γ_0 and τ can all be directly obtained experimentally. The amplitude of the shear strain, γ_0 is evaluated by fitting a sinusoidal function to the recorded shear strain data. The linear shear modulus G is obtained by fitting a linear stress-strain relation to the stress-strain curves. In all cases, the relaxation time τ is obtained by fitting the normal

stress relaxation curves versus time to Eq. (21), as shown in Fig. 2. The results are plotted versus $1/(G\xi^2)$, to test the predicted scaling ξ and G. The mesh size for fibrin samples has been measured (see SI pore size analysis), while for PAAm we use a mesh size of 10 nm, consistent with prior literature [10] and the predicted $\tau \sim \eta d^2/G\xi^2$ using $G = 141$Pa, $\eta = 10^{-3}$Pa and $d \simeq 1$mm. For fibrin gels polymerized at 27° C, we find an average relaxation time $\tau = 12.5$s and $G = 3150$ Pa. We apply frequencies in the range 0.001 Hz to 1 Hz. In Fig. S1, the fit parameters from the two-fluid model are plotted versus frequency. In Fig. 3 of the main text, we have chosen three frequencies (0.001, 0.01 and 1 Hz) out of this frequency range, to show how the normal stress response changes from extensile to contractile behavior with changing frequency.

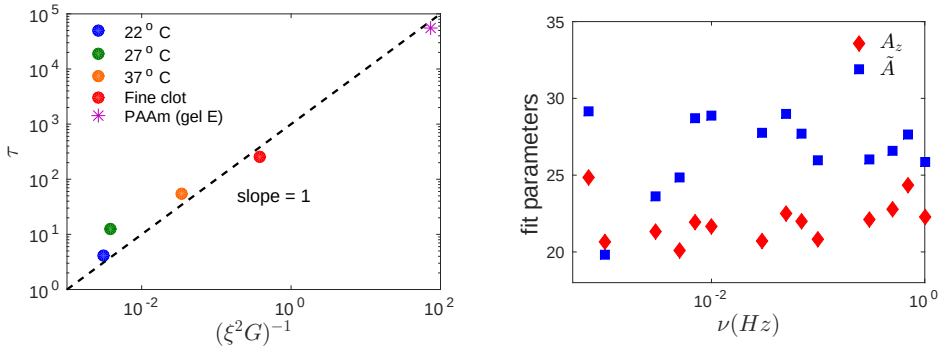

Supplementary Figure 1: a) Relaxation times for fibrin and PAAm gels are obtained from the fits in Fig. 2 of main text. These relaxation times are plotted vs $1/(G\xi^2)$ for comparison with predicted relaxation time dependence on ξ and G. For fibrin gels see SI pore size analysis below. For PAAm, we use $\xi = 10$nm, which is consistent both with prior literature values [10] and with the estimated $\xi \sim \sqrt{\eta d^2/(G\tau)}$ using our model, together with the fit $\tau = 15.5$h, $G = 141$Pa, $\eta = 10^{-3}$Pa and $d = R\tan(\alpha) = 25\tan(2^\circ)$mm $\simeq 1$mm. Fit parameters (A_z and $\tilde{A}$) for the fibrin sample polymerized at 27°C versus frequency.

Transient regime during oscillatory shear measurements

To measure the transition time in a fibrin gel polymerized under fine clot conditions (pore size 0.08 μm), we applied an oscillatory shear stress and measured the normal force as a function of time. Fig. S2 shows the transient regime, where the normal stress relaxes from a positive to a negative value over a characteristic time scale τ. This relaxation is similar ($\tau = 100$ s) to what is observed for experiments where a constant shear stress is applied (as shown in the main text in Figure 2).

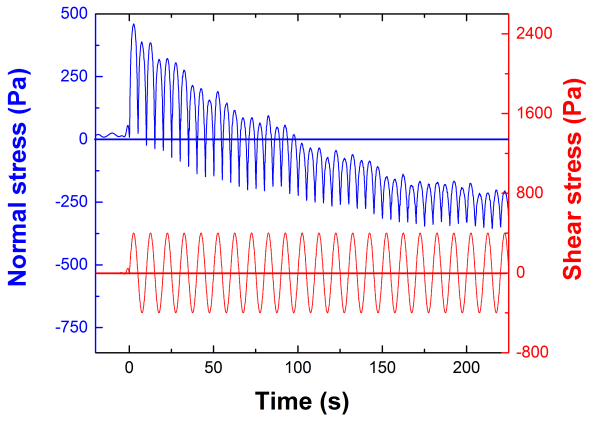

Supplementary Figure 2: Transient from a positive to a negative normal force for a fibrin gel, polymerized under fine clotting conditions, under oscillatory shearing ($f = 0.1Hz, \sigma = 400Pa$)

Influence of rheometer shear cell geometry on the normal stress signal

In this section, we show normal stress measurements obtained by shearing fibrin gels polymerized at 27 °C with different geometries. The dimensional analysis explained in the section 'Two-fluid model and relaxation of hoop stress' predicts that the characteristic time constant of the gel should scale as $\tau \sim \frac{\eta d^2}{G\xi^2}$ (Eq. (5)), where d is a characteristic length scale of the problem. By changing the measurement geometries, we thus expect the normal force signal at a given frequency to change.

We measure for different frequencies the phase shift ϕ between the normal force signal, $N(t) = A\cos(2.(2\pi\nu)t + \phi)$, and the squared shear strain, $\gamma(t)^2 = (\gamma_0 \cos((2\pi\nu).t))^2 = \frac{\gamma_0^2}{2}(1 + \cos(2.(2\pi\nu).t)$. We choose to compare $N(t)$ with $\gamma(t)^2$ because both quantities have the same frequency (2ν), and because of the analogy with the Mooney-Rivlin model prediction, $N = G\gamma^2$. The phase shift as a function of frequency measured for several plate-plate (PP) geometries and cone-plate (CP) geometries is shown in Fig. S3. We observe a marked dependence on gap size and cone angle.

As shown in Fig. 3b, we can scale out these differences by rescaling the frequency axis by the characteristic relaxation time $\tau \sim \frac{\eta d^2}{(G\xi^2)}$, where η is the viscosity of the interstitial fluid (10^{-3} Pa s), G is the storage modulus of the gel (which varies slightly with each experiment), d is the gap of the rheometer (chosen at the edges for the cone-plate geometries) and ξ is the mesh size of the gel (0.29 μm at 27°C). We observe a collapse of all the curves (Fig. 3b), showing that the gap size is the relevant length scale that governs the time-dependence of the normal force, in accordance with predictions from the dimensional analysis.

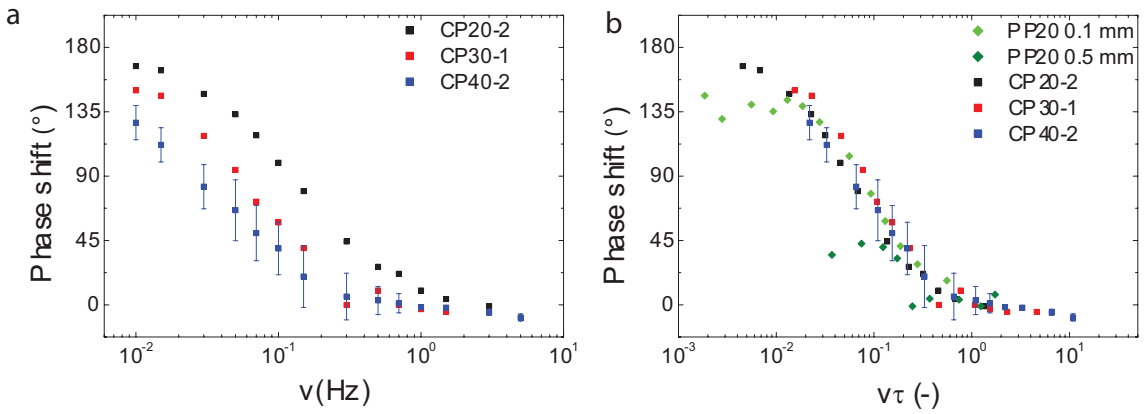

Supplementary Figure 3: **a**: Apparent phase shift between the normal stress and the shear strain for fibrin gels polymerized at 27°C as a function of the shearing frequency, for various shearing geometries. **b**: The frequency axis is rescaled by the characteristic time $\tau \sim \eta d^2/(G\xi^2)$. Error bars on the CP40-2 data set represent the standard deviation between 6 measurements.

Pore size analysis

The pore size of the fibrin gels was determined using turbidimetry, and verified by confocal microscopy. Turbidimetry data was analyzed based on a model for light scattering from isotropic networks of rigid rods [2, 3] in order to obtain the average mass-length ratio of the fibrin fibers. The fiber density in terms of the total length per volume, ρ, was calculated from the mass-length ratio and the fibrinogen mass concentration; we then obtained the mesh size $\xi \sim \sqrt{1/\rho}$.

An independent way to obtain the gel's pore size is through analysis of confocal images [11]. Analysis was done on 2 independently polymerized samples. Planes were analyzed separately. A FFT bandpass filter was applied to each confocal plane, filtering out features smaller than 2 pixels and larger than 30 pixels. As fibers were typically 5 pixels in diameter, this filtering step preserves their structure. Various thresholding techniques were applied: the built-in Matlab thresholding function (imgbw), Kapur's thresholding method (also known as the Maximum Entropy method) [12] and Otsu's thresholding method [13]. An overview of images with the FFT filter and thresholding applied is shown in Figure S4. The pore sizes obtained using analysis of turbidity spectra and image analysis are shown in Table 1. Although absolute values differ, the ratios between the 22°C and the 27°C show a consistent picture where the pore size of the fibrin network decreases upon an increase in the polymerization temperature by a factor of approximately 1.2. A histogram of the resulting pore size distributions is shown in Figure S5.

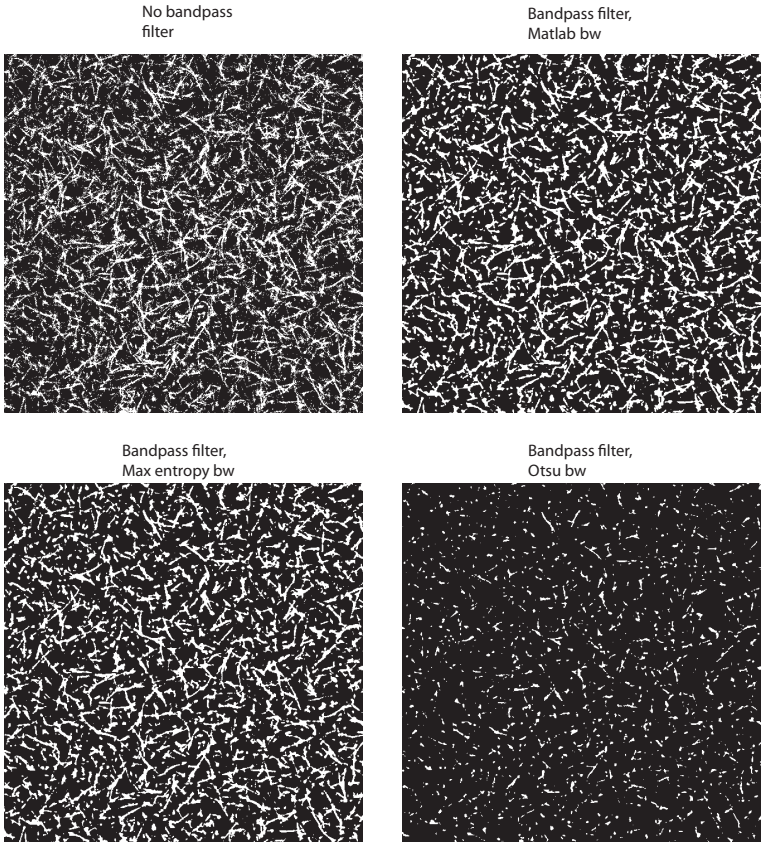

Supplementary Figure 4: Various thresholding methods (Matlab's default thresholding function, Kapur's or Maximum Entropy method [12], Otsu's method [13]) applied on the same confocal plane, without (top left) or with a FFT bandpass filter. Images are 40 by 40 μm.

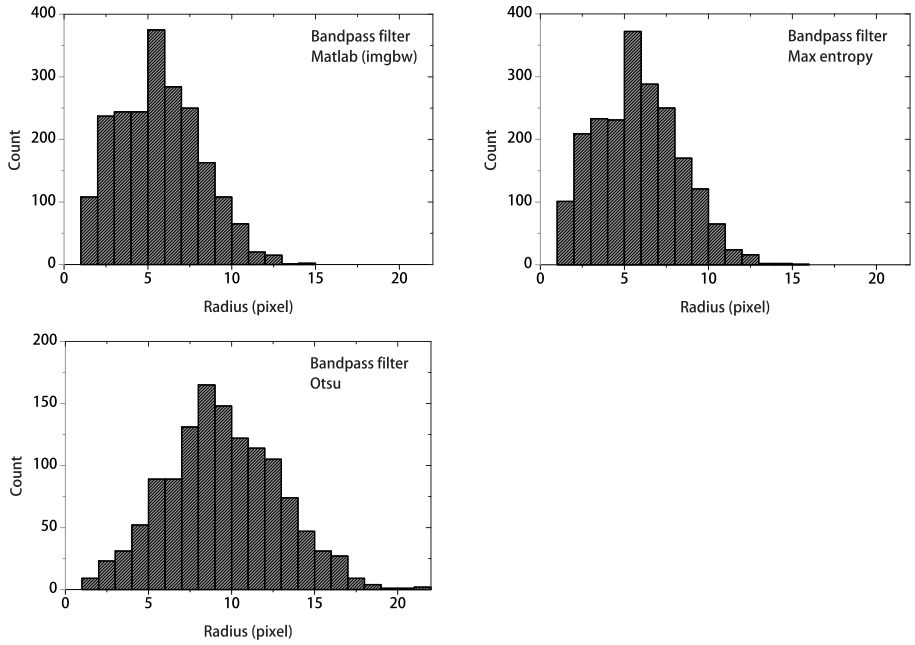

Supplementary Figure 5: Pore size distribution resulting from bubble analysis as described in [11], applied on images that are thresholded using various methods.

	22°C, pore size (μm)	27°C, pore size (μm)	Ratio
BP filter, Matlab (imgbw)	0.66 (0.00)	0.54 (0.03)	1.21
BP filter, Max. entropy	0.68 (0.01)	0.60 (0.03)	1.12
BP filter, Otsu	1.19 (0.10)	0.92 (0.12)	1.29
Photospectrometry	0.36 (0.01)	0.29 (0.01)	1.24

Table 1: Pore sizes in μm of 8 mg/ml fibrin gels polymerized at 22°C and 27°C, obtained using bubble analysis of confocal images with various thresholding methods, and turbidimetry. The number between brackets is the standard deviation between measurements.

References

[1] M. D. Bale, M. F. Müller, and J. D. Ferry, "Effects of fibrinogen-binding tetrapeptides on mechanical properties of fine fibrin clots.," *Proceedings of the National Academy of Sciences of the United States of America*, vol. 82, no. 5, pp. 1410–3, 1985.

[2] C. Yeromonahos, B. Polack, and F. Caton, "Nanostructure of the fibrin clot.," *Biophysical journal*, vol. 99, pp. 2018–27, oct 2010.

[3] I. K. Piechocka, K. A. Jansen, C. P. Broedersz, N. A. Kurniawan, F. C. MacKintosh, and G. H. Koenderink, "Multi-scale strain-stiffening of semiflexible bundle networks.," *Soft matter*, vol. 12, pp. 2145–2156, 2016.

[4] F. Brochard and P. G. de Gennes, "Dynamical Scaling for Polymers in Theta Solvents," *Macromolecules*, vol. 10, pp. 1157–1161, Sept. 1977.

[5] S. T. Milner, "Dynamical theory of concentration fluctuations in polymer solutions under shear," *Physical Review E*, vol. 48, pp. 3674–3691, Nov. 1993.

[6] F. Gittes, B. Schnurr, P. D. Olmsted, F. C. MacKintosh, and C. F. Schmidt, "Microscopic viscoelasticity: Shear moduli of soft materials determined from thermal fluctuations," *Phys. Rev. Lett.*, vol. 79, pp. 3286–3289, Oct 1997.

[7] A. J. Levine and T. C. Lubensky, "One- and Two-Particle Microrheology," *Physical Review Letters*, vol. 85, pp. 1774–1777, Aug. 2000.

[8] P. A. Janmey, M. E. McCormick, S. Rammensee, J. L. Leight, P. C. Georges, and F. C. MacKintosh, "Negative normal stress in semiflexible biopolymer gels.," *Nature materials*, vol. 6, pp. 48–51, Jan. 2007.

[9] H. Kang, Q. Wen, P. a. Janmey, J. X. Tang, E. Conti, and F. C. MacKintosh, "Nonlinear elasticity of stiff filament networks: Strain stiffening, negative normal stress, and filament alignment in fibrin gels," *Journal of Physical Chemistry B*, vol. 113, pp. 3799–3805, 2009.

[10] M. Tombs, "The interpretation of gel electrophoresis," *Analytical Biochemistry*, vol. 13, no. 1, pp. 121–132, 1965.

[11] S. Münster and B. Fabry, "A Simplified Implementation of the Bubble Analysis of Biopolymer Network Pores," *Biophysical Journal*, vol. 104, no. 12, pp. 2774–2775, 2013.

[12] J. Kapur, P. Sahoo, and A. Wong, "A new method for gray-level picture thresholding using the entropy of the histogram," *Computer Vision, Graphics, and Image Processing*, vol. 29, pp. 273–285, mar 1985.

[13] N. Otsu, "A Threshold Selection Method from Gray-Level Histograms," *IEEE Transactions on Systems, Man, and Cybernetics*, vol. 9, pp. 62–66, nov 1979.